batteries

MDPI

Article

Synthesis and Electrochemical Performance of Ni-Doped VO_2(B) as a Cathode Material for Lithium Ion Batteries

Qian Yang, Zhengguang Zou *, Xingyu Wu, Shengyu Li and Yanjiao Zhang

College of Materials Science and Engineering, Guilin University of Technology, Guilin 541000, China; ysyangqian0539@163.com (Q.Y.); wuxingyu163@163.com (X.W.); LSYLGDX@163.com (S.L.); zhangyanjiao154@163.com (Y.Z.)

* Correspondence: zouzgglut@163.com or zouzg@glite.edu.cn

Received: 16 March 2019; Accepted: 20 May 2019; Published: 1 June 2019

Abstract: Ni-doped VO_2(B) samples (Ni_xVO_2(B)) were fabricated by a facile one-step hydrothermal method. When evaluated as a cathode material for lithium ion batteries (LIBs), these Ni-doped VO_2(B) exhibited improved lithium storage performance as compared to the pure VO_2(B). In particular, when the doping amount is 3%, Ni_xVO_2(B) showed the highest lithium storage capacity, best cycling stability, smallest electrochemical reaction resistance, and largest lithium diffusion coefficient. For example, after 100 cycles at a current density of 32.4 mA/g, Ni_xVO_2(B) delivered a high specific discharge capacity of 163.0 mAh/g, much higher than that of the pure VO_2(B) sample (95.5 mAh/g). Therefore, Ni doping is an effective strategy for enhancing the lithium storage performance of VO_2(B).

Keywords: lithium ion batteries; cathode material; Ni doping; VO_2(B); electrode materials; energy storage and conversion

1. Introduction

Rechargeable lithium-ion batteries (LIBs) have been widely used as power sources for portable electronics, electric vehicles (EV), and hybrid vehicles (HEV) [1–3]. To meet the ever-increasing demand of high energy density LIBs, it is very crucial to develop high-capacity electrode active materials [4,5]. Among the various candidate cathode materials, vanadium oxides have attracted great attentions due to their high energy density, low cost, and abundant sources [6,7]. In particular, metastable mono-clinic VO_2(B) stands out from these vanadium oxides because of its unique VO_2(B) bilayer structure, large lattice spacing of edge-sharing VO_6 octahedron, high theoretical capacity, and fast ion-transfer rate [8,9]. Unfortunately, the practical capacity of VO_2(B) is significantly lower than its theoretical capacity (324 $mAh{\cdot}g^{-1}$) and the cycling stability is poor. To solve these issues, many strategies, such as nanocrystallization [9–11] and carbonization [12,13], were adopted and these materials indeed exhibit improved electrochemical performance. However, the cycling performance is still not satisfied enough for practical applications, due to collapse of the active material and the increased charge transfer resistance upon repeated cycling [10–13].

It has been demonstrated doping alien metal cations could enhance the structural stability and improve the electrical conductivity of electrode materials, which are crucial parameters for determining the cyclability of electrodes [14,15]. Hou et al. synthesized Al^{3+} doped VO_2(B), which delivered a high initial discharge capacity (282 mAh/g at 32.4 mA/g) and high capacity retention rate (71.6% after 50 cycles) [16]. Han et al. reported Ag^+ doped VO_2(B); this Ag^+ doped VO_2(B) delivered higher initial discharge capacity (340.5 mAh/g at 32.4 mA/g), which was 151.9 mAh/g higher than the undoped one; but the capacity retention rate was only 27.1% after 100 cycles, significantly lower than the undoped

one (41.6%) [17]. Since the ion radius of Ni^{2+} (0.055 nm) is very close to that of V^{4+} (0.058 nm), Ni^{2+} can easily enter the lattice of VO_2(B) and substitute V^{4+}, resulting in oxygen vacancies and improved rate performance. Therefore, Ni^{2+} was doped in $LiFeBO_3$/C, $Na_3V_2(PO4)_3$/C, $LiMn_2O_4$, MnO_2/CNT and other cathode materials to improve their electrochemical performance [18–20]. It should be noted that there are few reports on Ni-doped VO_2(B).

Herein, Ni^{2+} doped VO_2(B) was successfully synthesized from V_2O_5, nickel nitrate, and maltose by a facile hydrothermal method. The effect of Ni^{2+} doping on the microstructure and electrochemical properties of VO_2(B) were investigated by XRD, SEM, cyclic voltammetry (CV), electrochemical impedance spectroscopy (EIS), and charge/discharge tests.

2. Experimental

2.1. Synthesis of Ni-Doped VO_2(B)

Metastable VO_2(B) was synthesized by a hydrothermal method. Vanadium oxide (V_2O_5) powder was used as the V source and maltose ($C_{12}H_{22}O_{11}$) as the deoxidizer. All the chemical reagents were analytical grade

In a typical process, 0.5 g V_2O_5 powders, 0.25 g$C_{12}H_{22}O_{11}$, and a proper amount of nickel nitrate ($Ni(NO_3)_2$) were dissolved in 50 mL deionized water. The Ni/V molar ratio was controlled to be 0 at.%, 1 at.%, 2 at.%, 3 at.% and 4 at.%, respectively. After magnetic stirring at room temperature for 0.5 h, the mixed solution was transferred to an autoclave and heated at 180 °C for 24 h in an oven. After hydrothermal reaction, the resulting precipitate was collected by filtration, freeze-dried, and sintered at 350 °C for 1 h in nitrogen atmosphere to yield Ni^{-}doped VO_2(B) samples. The samples with Ni/V molar ratio of 0 at.%, 1 at.%, 2 at.%, 3 at.% and 4 at.% were labeled as Ni0, Ni1, Ni2, Ni3, and Ni4, respectively.

2.2. Characterization

The phase structure of the samples was determined by X-ray powder diffraction (XRD, Rigaku RINT2400 with Cu Kα radiation), at a scan rate of 20°/min. The surface morphology of the samples was observed by a field emission scanning electron microscope (S-4800, Japan Hi-Tech Corporation, Tokyo, Japan). The composition of the samples was analyzed by an energy diffusion spectrometer (EDS, Oxford, UK, INCA IE 350).

2.3. Electrochemical Tests

The electrochemical performance of the samples were evaluated in coin-type cells (CR2025), which were assembled in a Mikrouna glove box filled with high purity argon. The working electrodes were fabricated by coating the slurry of Ni-doped VO_2(B), acetylene black, and polyvinylidene fluoride (PVDF) binder with a weight ratio of 7:2:1 dispersed in N-Methyl-2-pyrrolidone solvent on an aluminum foil. The obtained electrodes were then dried in a vacuum of 90 °C for 12 h and punched to the disks with the diameter of 16 mm. Lithium foil was used as the anode electrode and single layer polypropylene (PP) as the separator. 1 mol/L LiPF6 in a mixture solution of ethylene carbonate (EC), dimethyl carbonate (DMC), diethyl carbonate (DEC) ($v/v/v$ = 1:1:1) was used as electrolyte.

Galvanostatic discharge/charge measurement was performed in a voltage range of 1.5–4.0 V (vs. Li/Li^{+}). Both the electrochemical impedance spectroscopy (EIS) and the cyclic voltammetry (CV) were carried out using a CHI760D electrochemical workstation.

3. Results and Discussion

Figure 1 presents the XRD patterns of the series of Ni-doped VO_2(B) samples. It can be seen that the diffraction peaks of all the samples match well with the standard card of VO_2(B) (JCPDS No. 81-2392). No peaks of other phases or impurities were observed, implying that Ni^{2+} doping did not change the phase structure of VO_2(B). By a careful observation (shown in Figure 1b), one can see that the (110) diffraction peak shifts toward high angle with the increasing Ni^{2+} doping content. This

change is likely due to the difference of ionic radius of Ni^{2+} (0.055 nm) and V^{4+} (0.058 nm). After doping, Ni^{2+} cations entered the crystal lattice and substitutes V^{4+}, which changed the interplanar spacing and therefore leading to the shift of diffraction peaks. This verified that Ni^{2+} cations have been successfully incorporated into the VO_2(B) lattice.

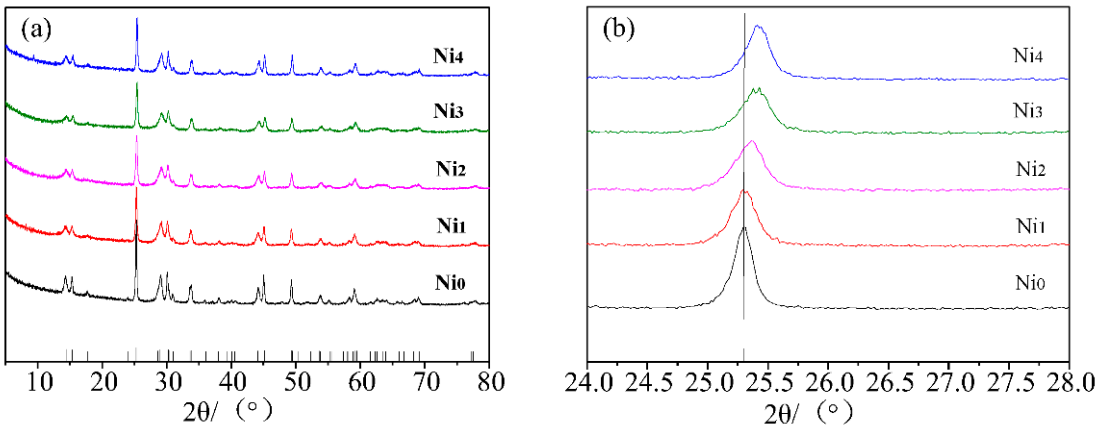

Figure 1. (**a**) XRD patterns of the Ni_0, Ni_1, Ni_2, Ni_3, and Ni_4 samples. (**b**) Local magnified XRD patterns from 24° to 28°.

In order to study the actual element composition of the series of Ni-diped VO_2(B), we performed EDS analysis on the samples and the results are listed in Table 1. It can be seen that the Ni content in the samples increased with the increasing amount of $Ni(NO_3)_2$ during hydrothermal process. This also verified that Ni^{2+} cations were successfully doped into the VO_2(B) lattice. However, the actual Ni/V molar ratio in the samples was smaller the initial Ni/V molar ratio in the reaction solutions.

Table 1. The theoretical atomic percentage and actual atomic percentage of the samples.

Sample Designation	Ni:V Atomic Percentage (Starting Composition)	Ni:V Atomic Percentage (Actual Composition)
Ni_0	0	0
Ni_1	1%	0.45%
Ni_2	2%	0.66%
Ni_3	3%	1.50%
Ni_4	4%	1.80%

Figure 2 gives the SEM images of the Ni_0, Ni_1, Ni_2, Ni_3, and Ni_4 samples. All the samples had a rod-like morphology. After Ni-doping, the diameter of the VO_2(B) rod slightly decreased compared to the undoped sample, suggesting that the growth of the VO_2(B) crystal was suppressed. In particular, the size of the Ni_3 sample (with length in the range of 1–1.5 μm) was nearly half the length of the Ni_0 sample (in the range of 1–3 μm); in addition, the particle size of Ni_3 sample was more uniform than that of the Ni_0 sample. The uniform and smaller size of Ni_0 could provide a larger specific surface area [21], facilitate the transport of Li^+ [22], and improve the electrochemical performance of the material.

Figure 3a shows the cycling performances of the series of samples at a current density of 32.4 mA/g. The first specific discharge capacities of Ni_0, Ni_1, Ni_2, Ni_3, Ni_4 were 216, 227, 228, 251, and 246 mAh/g, respectively. After 100 cycles, the corresponding specific capacities decreased to 95.5, 137.0, 163.0, 134.8, and 110.5 mAh/g, respectively; the capacity retention rates were 44.2%, 48.7%, 59.1%, 64.9%, and 55.7% for of Ni_0, Ni_1, Ni_2, Ni_3, and Ni_4, respectively. Generally, this capacity decay is mainly caused by the collapse of the crystal structure of VO_2(B), which hinders the intercalation/de-intercalation of Li^+ during discharge/charge cycles. Obviously, the Ni doping increased first discharge capacity and improved the capacity retention rate of VO_2(B). That is, Ni^{2+} doping into can increase the structural

stability of the V–O bond, thus stabilizing the crystal structure of VO_2(B) and increasing the capacity retention rate. At the same time, the substitution of Ni^{2+} for V^{4+} in VO_2(B) can generate additional oxygen vacancies, which can broaden the channels for the diffusion of lithium ions. Among the five samples, Ni_3 had the best lithium storage performance. With the increase of Ni doping amount, the first specific discharge capacity and capacity retention rate first increased and then decreased, indicating that an appropriate amount of Ni^{2+} doping can improve the electrochemical performance of VO_2(B). For the Ni_4 sample, the excessive substitution of Ni^{2+} for V^{4+} made the crystal lattice of VO_2(B) excessively deformed and unstable, and therefore hindered the diffusion of Li^+. Figure 3b–f are the typical charge/discharge curves of Ni_0, Ni_1, Ni_2, Ni_3, and Ni_4 samples in the 1st, 50th, and 100th cycle. All charge/discharge curves showed very similar features, having two distinct plateaus (2.5 V and 1.7 V), corresponding to lithium de-intercalation and intercalation reactions. Among them, the discharge plateau at 2.5 V corresponded to the reduction of V^{5+} to V^{4+} [23], and the discharge plateau at 2.2 V corresponded to the reduction of V^{4+} to V^{3+} [24]. The separation between the charge and discharge plateaus decreased significantly after Ni doping, demonstrating that the electrochemical polarization of the electrode was reduced and the capacity was increased.

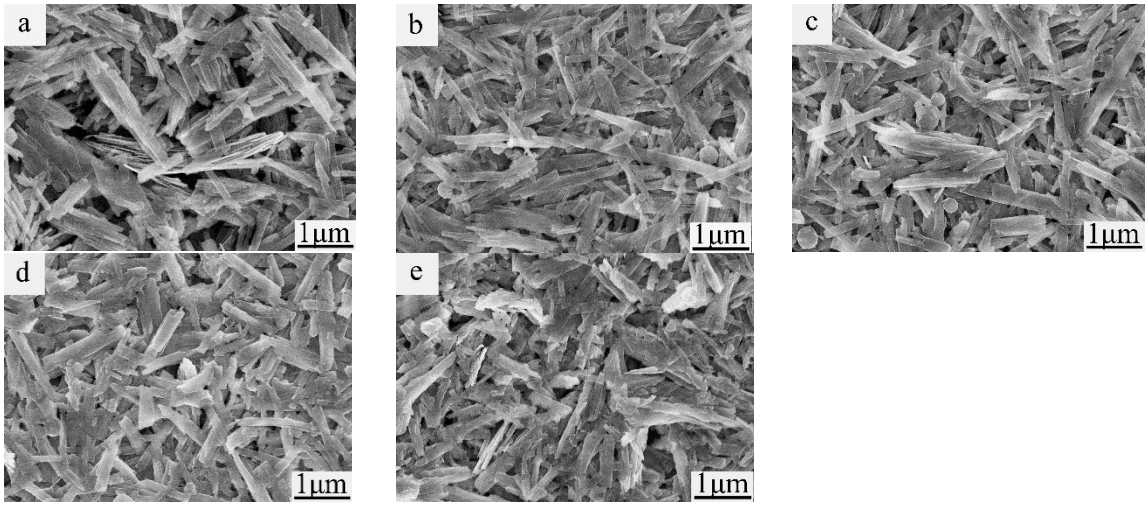

Figure 2. SEM images of (**a**) Ni_0, (**b**) Ni_1, (**c**) Ni_2, (**d**) Ni_3, and (**e**) Ni_4, respectively.

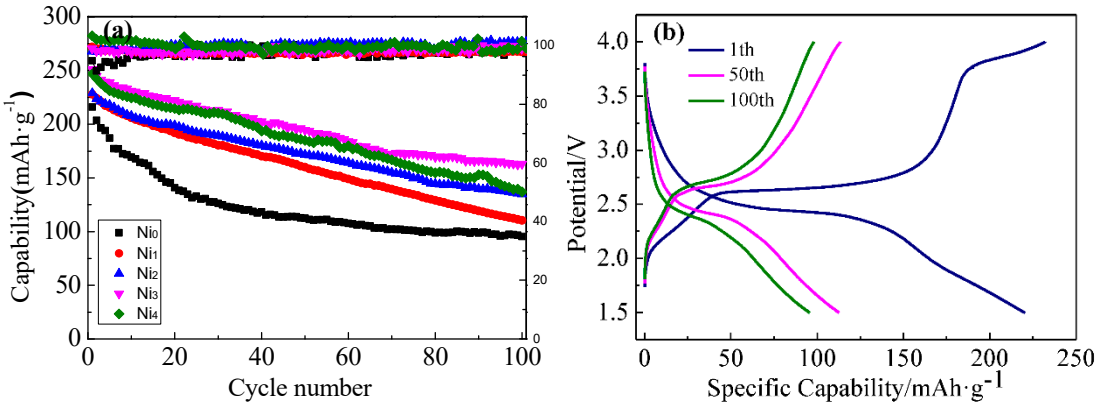

Figure 3. *Cont.*

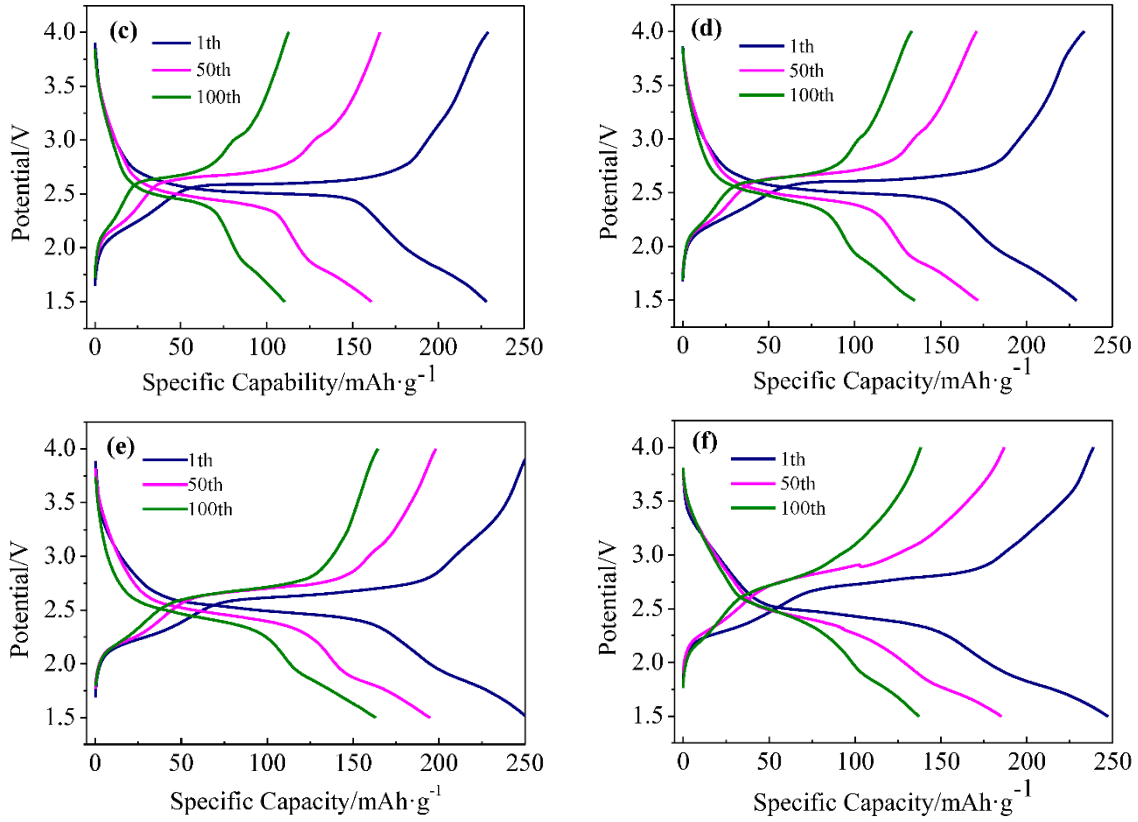

Figure 3. (**a**) Cycling performance and (**b**–**f**) selected charge/discharge curves of Ni_0, Ni_1, Ni_2, Ni_3, and Ni_4 samples at a current density of 32.4 mA/g.

Figure 4a shows the CV curve of the series of samples measured at a scan rate of 0.1 mV/s in the voltage of 1.5–4.0 V. All the samples clearly presented a couple of redox peaks, representing the process of the intercalation/de-intercalation of Li^+ [15]. With the increase of Ni doping amount, the oxidation peak reduction peak shifted to the lower potential side and higher potential side, respectively. This can be attributed to the structural change and depolarization after Ni doping [12]. The potential difference between oxidation peak and reduction peak ($\Delta\varphi$) of Ni_0, Ni_1, Ni_2, Ni_3, and Ni_4 were 0.99 V, 0.92 V, 0.54 V, 0.58 V, and 0.88 V, respectively. It is obvious that the potential difference decreased after Ni doping, which is indicative of decreased electrochemical polarization and better electrochemical reaction reversibility of the electrodes [25].

To investigate the electrochemical reaction kinetics of the electrode, EIS plots were tested after the electrodes were activated for three cycles, and the results are shown in Figure 4b. The charge transfer resistances of Ni_0, Ni_1, Ni_2, Ni_3, and Ni_4 were 860.0 Ω, 718.2 Ω, 615.0 Ω, 542.9 Ω, and 636.0 Ω, respectively. Obviously, the charge transfer resistance of VO_2(B) was decreased after Ni doping. That is, the substitution of Ni^{2+} for V^{4+} in VO_2(B) can effectively enhance the electrochemical reaction in VO_2(B) [22]. As shown in Figure 2, the Ni doped samples had a larger specific surface area, which can increase the electrochemical active sites and benefit the fast intercalation and deintercalation of Li^+ [26]. To further understand the Li^+ diffusion performance of the samples, Figure 4c gives the relationship between Z' and $\omega^{-1/2}$ according to the EIS plots in Warburg region. The lithium ion diffusion coefficient of the samples can be evaluated according to the following formula [27,28]:

$$D_{Li} = \frac{(RT)^2}{2\left(An^2F^2C_{Li}\sigma\right)^2} \quad (1)$$

where A is the surface area of the electrode and n is the number of electrons per mole in the oxidation reaction; F is the Faraday constant; C_{Li} is the concentration of Li^+; σ is the Warburg coefficient, which can be obtained from the slope of Z′ vs. $\omega^{-1/2}$ in Warburg region (Figure 4c); R is the gas constant; and T is kelvin degree (298 K).

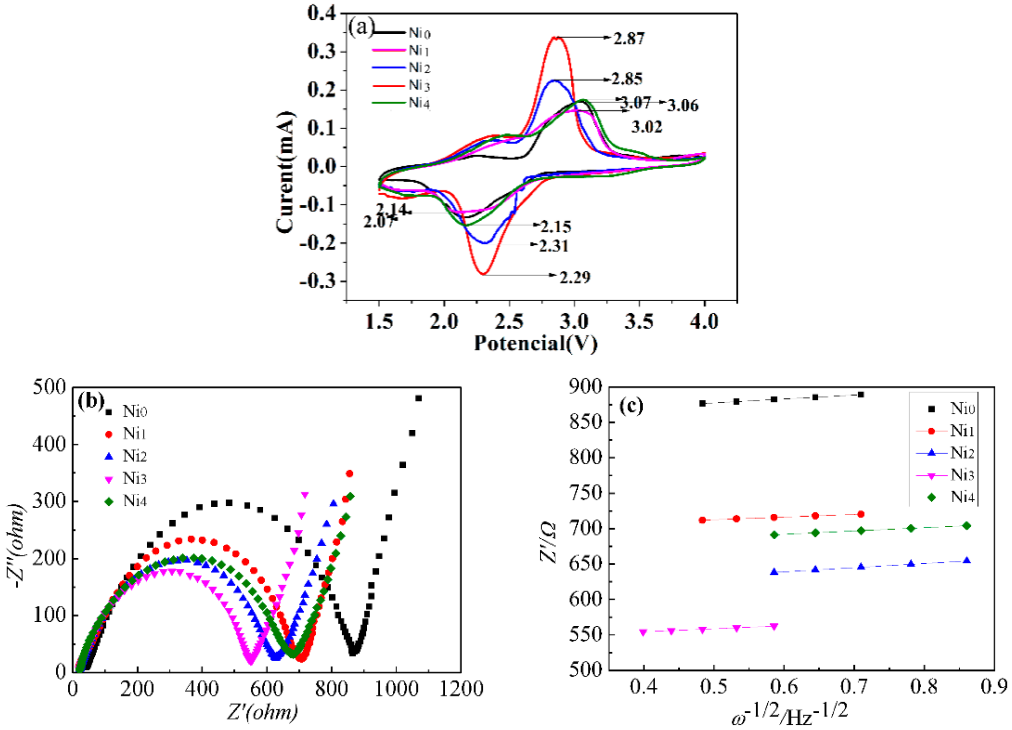

Figure 4. (**a**) Cycle voltammetry (CV) curves of Ni_0, Ni_1, Ni_2, Ni_3 and Ni_4 samples. (**b**) The electrochemical impedance spectroscopy (EIS) plots of Ni_0, Ni_1, Ni_2, Ni_3 and Ni_4 samples after three discharge/charge cycles. (**c**) The relationship between Z′ and $\omega^{-1/2}$ obtained from EIS plots shown in (**b**).

The calculated lithium ion diffusion coefficients of Ni_0, Ni_1, Ni_2, Ni_3, Ni_4 were 2.82×10^{-15}, 4.426×10^{-15}, 5.24×10^{-15}, 6.815×10^{-15}, 3.13×10^{-15} cm^2/s, respectively (Table 2). Apparently, the lithium ion diffusion coefficient increased after Ni doping, and Ni_3 had the largest lithium ion diffusion coefficient among the five samples.

Table 2. σ and D_{Li} values of the samples.

Sample Designation	σ	D_{Li}
Ni_0	58.2773	2.82×10^{-15}
Ni_1	46.5196	4.426×10^{-15}
Ni_2	42.7479	5.24×10^{-15}
Ni_3	37.4864	6.815×10^{-15}
Ni_4	55.2987	3.13×10^{-15}

4. Conclusions

In this work, Ni-doped VO_2(B) samples were synthesized by a hydrothermal method. The effect of Ni doping amount on the microstructure and lithium storage performance was investigated in detail. It was found that Ni doping facilitates the formation of uniform and smaller rod-like VO_2(B). Electrochemical performance tests demonstrated that Ni doping can increase the lithium ion diffusion coefficient, reduce the electrochemical reaction resistance and polarization of VO_2(B) electrode during charge/discharge process. In particular, when the doping amount was 3%, the sample exhibited the

best lithium storage performance. After 100 cycles at a current density of 32.4 mA/g, this sample delivered a specific discharge capacity of 163.0 mAh/g, much higher than that of the pure VO_2(B) sample (95.5 mAh/g). The results reported in this work could provide clues for the rational structural design and performance optimization of vanadium oxides cathode materials.

Author Contributions: Conceptualization, Q.Y., Z.Z.; methodology, data treating and writing—original draft preparation, Q.Y.; Article inspection and approval, Z.Z. and X.W.; experiment, Q.Y., X.W., S.L. and Y.Z.

Funding: This research was funded by National Natural Science Foundation of China (Grant Number 51562006).

Acknowledgments: This work was supported by the National Nature Science Foundation of China (No. 51562006).

Conflicts of Interest: The authors declare no conflict of interest.

References

1. Harks, P.P.R.M.L.; Mulder, F.M.; Notten, P.H.L. In situ methods for Li-ion battery research: A review of recent developments. *J. Power Sources* **2015**, *288*, 92–105. [CrossRef]
2. Goodenough, J.B.; Park, K.S. The Li-ion rechargeable battery: A perspective. *J. Am. Chem. Soc.* **2013**, *135*, 1167–1176. [CrossRef] [PubMed]
3. Xu, J.; Lin, F.; Doeff, M.M.; Tong, W. A review of Ni-based layered oxides for rechargeable Li-ion batteries. *J. Mater. Chem. A* **2017**, *5*, 874–901. [CrossRef]
4. Yang, Z.; Zhang, J.; Kintner-Meyer, M.C.; Lu, X.; Choi, D.; Lemmon, J.P.; Liu, J. Electrochemical energy storage for green grid. *Chem. Rev.* **2011**, *111*, 3577–3613. [CrossRef] [PubMed]
5. Huie, M.M.; Bock, D.C.; Takeuchi, E.S.; Marschilok, A.C.; Takeuchi, K.J. Cathode materials for magnesium and magnesium-ion based batteries. *Coord. Chem. Rev.* **2015**, *287*, 15–27. [CrossRef]
6. Li, H.; He, P.; Wang, Y.; Hosono, E.; Zhou, H. High-surface vanadium oxides with large capacities for lithium-ion batteries: from hydrated aerogel to nanocrystalline VO_2(B), V_6O_{13} and V_2O_5. *J. Mater. Chem.* **2011**, *21*, 10999–11009. [CrossRef]
7. Ding, N.; Feng, X.; Liu, S.; Xu, J.; Fang, X.; Lieberwirth, I.; Chen, C. High capacity and excellent cyclability of vanadium (IV) oxide in lithium battery applications. *Electrochem. Commun.* **2009**, *11*, 538–541. [CrossRef]
8. Yan, B.; Li, X.; Bai, Z.; Lin, L.; Chen, G.; Song, X.; Xiong, D.; Li, D.; Sun, X. Superior sodium storage of novel VO_2 nano-microspheres encapsulated into crumpled reduced graphene oxide. *J. Mater. Chem. A* **2017**, *5*, 4850–4860. [CrossRef]
9. Niu, C.; Meng, J.; Han, C.; Zhao, K.; Yan, M.; Mai, L. VO2 nanowires assembled into hollow microspheres for high-rate and long-life lithium batteries. *Nano Lett.* **2014**, *14*, 2873–2878. [CrossRef]
10. Reddy, C.V.S.; Walker, E.H., Jr.; Wicker, S.A., Sr.; Williams, Q.L.; Kalluru, R.R. Synthesis of VO_2 (B) nanorods for Li battery application. *Curr. Appl. Phys.* **2009**, *9*, 1195–1198. [CrossRef]
11. Mai, L.; Wei, Q.; An, Q.; Tian, X.; Zhao, Y.; Xu, X.; Xu, L.; Chang, L.; Zhang, Q. Nanoscroll Buffered Hybrid Nanostructural VO_2 (B) Cathodes for High-Rate and Long-Life Lithium Storage. *Adv. Mater.* **2013**, *25*, 2969–2973. [CrossRef]
12. Zhao, Q.; Jiao, L.; Peng, W.; Gao, H.; Yang, J.; Wang, Q.; Du, H.; Li, L.; Qi, Z.; Si, Y.; et al. Facile synthesis of VO_2 (B)/carbon nanobelts with high capacity and good cyclability. *J. Power Sources* **2012**, *199*, 350–354. [CrossRef]
13. Wang, F.; Liu, Y.; Liu, C.Y. Hydrothermal synthesis of carbon/vanadium dioxide core–shell microspheres with good cycling performance in both organic and aqueous electrolytes. *Electrochim. Acta* **2010**, *55*, 2662–2666. [CrossRef]
14. Liu, G.; Du, Y.; Liu, W.; Wen, L. Study on the action mechanism of doping transitional elements in spinel $LiNi_{0.5}Mn_{1.5}O_4$. *Electrochim. Acta* **2016**, *209*, 308–314. [CrossRef]
15. Fang, D.L.; Li, J.C.; Liu, X.; Huang, P.F.; Xu, T.R.; Qian, M.C.; Zheng, C.H. Synthesis of a Co–Ni doped $LiMn_2O_4$ spinel cathode material for high-power Li-ion batteries by a sol–gel mediated solid-state route. *J. Alloys Compd.* **2015**, *640*, 82–89. [CrossRef]
16. Zou, Z.G.; Hou, Z.L.; Wang, J.L.; Gao, Y.; Wan, Z.D. Hydrothermal Synthesis and Electrochemical Performance of Al-doped VO_2(B) as Cathode Materials for Lithium-Ion Battery. *Int. J. Electrochem. Sci.* **2017**, *12*, 4979–4989. [CrossRef]

17. Han, S.C.; Zou, Z.G.; Lv, T.T.; Wu, X.Y.; Yang, Q. Synthesis and electrochemical performance of Ag- doped VO_2(B) as cathode materials. *CIESC J.* **2018**, *69*, 1741–1748.
18. Zhang, B.; Ming, L.; Tong, H.; Zhang, J.F.; Zheng, J.C.; Wang, X.W.; Li, H.; Cheng, L. Ni-doping to improve the performance of $LiFeBO_3$/C cathode material for lithium-ion batteries. *J. Alloys Compd.* **2018**, *740*, 382–388. [CrossRef]
19. Zhang, B.; Chen, H.; Tong, H.; Wang, X.; Zheng, J.; Yu, W.; Zhang, J.; Li, J.; Zhang, W. Synthesis and electrochemical performance of Ni doped $Na_3V_2(PO_4)_3$/C cathode materials for sodium ion batteries. *J. Alloys Compd.* **2017**, *728*, 976–983. [CrossRef]
20. Asif, M.; Rashad, M.; Ali, Z.; Qiu, H.; Li, W.; Pan, L.; Hou, Y. Ni-doped MnO_2/CNT nanoarchitectures as a cathode material for ultra-long life magnesium/lithium hybrid ion batteries. *Mater. Today Energy* **2018**, *10*, 108–117. [CrossRef]
21. Yu, A.; Kumagai, N.; Liu, Z.; Lee, J.Y. A new method for preparing lithiated vanadium oxides and their electrochemical performance in secondary lithium batteries. *J. Power Sources* **1998**, *74*, 117–121. [CrossRef]
22. Liu, Y.C.; Wu, N.L.; Liu, W.R. Electrochemical Properties of Al^3+/Cl^- Doped-0.2Li_2MnO_3·0.8$LiNiO_2$ Cathode Materials for Lithium-Ion Batteries. *J. Nanosci. Nanotechnol.* **2018**, *18*, 68–74. [CrossRef]
23. Piffard, Y.; Leroux, F.; Guyomard, D.; Mansot, J.L.; Tournoux, M. The amorphous oxides MnV_2O_6 + δ (0 < δ < 1) as high capacity negative electrode materials for lithium batteries. *J. Power Sources* **1997**, *68*, 698–703.
24. Hu, F.; ZHANG, C.H.; Zhang, S.; Ming, X.; Chen, G.; WEI, Y.J.; WANG, C.Z. Electrochemical cycled structure of MnV_2O_6 nanoribbons synthesized via hydrothermal route. *Chem. Res. Chin. Univ.* **2011**, *27*, 528–530.
25. Yang, L.C.; Gao, Q.S.; Tang, Y.; Wu, Y.P.; Holze, R. MoO_2 synthesized by reduction of MoO_3 with ethanol vapor as an anode material with good rate capability for the lithium ion battery. *J. Power Sources* **2008**, *179*, 357–360. [CrossRef]
26. Huang, Y.; Lu, H.; Gu, H.; Fu, J.; Mo, S.; Wei, C.; Miao, Y.; Liu, T. A CNT@ $MoSe_2$ hybrid catalyst for efficient and stable hydrogen evolution. *Nanoscale* **2015**, *7*, 18595–18602. [CrossRef] [PubMed]
27. Liu, H.; Li, C.; Zhang, H.P.; Fu, L.J.; Wu, Y.P.; Wu, H.Q. Kinetic study on $LiFePO_4$/C nanocomposites synthesized by solid state technique. *J. Power Sources* **2006**, *159*, 717–720. [CrossRef]
28. Wang, L.L.; Sun, Z.Z.; Yi, W.T.; Ma, P.H. The Applications of EIS in the Research of $LiFePO_4$ as the Cathode Materials of Li-ion Batteries. *J. Salt Lake Res.* **2008**, *16*, 21–26.